IJES *Iranian Journal of Earth Sciences*
Vol. 12, No. 4, 2020, 292-302.

Detection of fault segments based on P–T dihedra analysis along the North Tabriz fault, NW Iran

Pouya Sadeghi-Farshbaf*[1], Mohammad Mahdi Khatib[1], Hamid Nazari[2]

1. Department of Geology, University of Birjand, Birjand, Iran
2. Research Institute for Earth Sciences, Tehran, Iran

Received 6 May 2019; accepted 17 April 2020

Abstract

Detection of fault segments is an essential step for tracking main transverse faults. General observations from field studies as well as attitude measurements can give an overall understanding of the lengths of the segments, but these are not always sufficient to accurately identify and characterize them. In this study, we analyze P–T dihedra variations based on their eigenvalues to detect fault segments. The anomalies of local paleostress distribution aid us to detect the segment boundaries. This study focuses on the Northwestern, Central, and Southeastern sectors of the North Tabriz Fault (NTF). Fault azimuth distribution and eigenvalue anomalies as well as the fault attitudes for each interval distance have been used to distinct segment boundaries. The results are verified by checking the presence of the transverse faults at the proposed sites during fieldwork. Results show a new structural arrangement integrated by the already documented NTF segments, combined with 6 related transverse faults. In this way, we confirm the earlier reported segments, and we improve the NFT characterization by introducing new segments bounded by transverse faults.

Keywords: *North Tabriz fault, Segmentation, Transverse fault, P–T dihedral, Paleostress*

1. Introduction

Fault–segment boundaries initiate, evolve and die as a result of the propagation, interaction and linkage of normal faults during crustal extension (Whipp et al. 2016). Fault segmentation and fault steps during their evolution are relevant to the dynamics and size of earthquake ruptures, the distribution of fault damage zones and the capacity of fault seal (de Joussineau and Aydin 2009). The identification and analysis of fault-segmentations is commonly used to estimate the potential earthquake size. Segment boundaries play an important role in detecting earthquake ruptures from event to event (Zhang et al. 1999). Segments are controlled by transverse faults and; therefore, fault segments detecting is an essential step for tracking main transverse faults. Understanding how natural faults are segmented along their length can provide useful insights into fault growth processes, stress distribution on fault planes, and earthquake dynamics (Manighetti et al. 2015). Another importance of segmentation study is to deduce tectonic stresses from numerical simulations based on segment lengths, orientations, and relative movements (e.g., Sadeghi-Farshbaf et al. 2019). The estimation of tectonic stresses is important for structural geologists for studies of geodynamic (Pollard 2000), foundation engineering (Amadei and Stephansson 1997), and subsurface fluid flow (Nelson 1985, Mandl 1999, Faulds et al. 2006, 2010, Huenges 2010). The basis of most of the segment detection methods consists of studying the connection between fault features, fault -segments boundaries (e.g., Walsh and Watterson 1991, Trudgill and Cartwright 1994, Mansfield and Cartwright 2001) and long-established faults (e.g., Manighetti et al. 2007, 2009). Other common methods include the integration of physical information (i.e. rupture length and displacement) about fault zone (e.g., Zhang et al. 1999) together with field observations (e.g., de Joussineau and Aydin 2009). However, the common factor of all the segment-detection methods consists in the field studies.

Our study area includes the total length of the NTF which is located in the western Alborz–Azerbaijan structural zone (WAASZ) in northwestern Iran (Nabavi 1976). Berberian (1997) divides the NTF into several segments that are identified according to a series of surface ruptures from the earthquakes of 1721, 1780, and 1786 AD. The NTF represents the central part of a large crustal fault system called the Tabriz Fault System (TFS) (Solaymani Azad et al. 2015). However, some scholars consider most of the Azerbaijan zone as belonging to the Central Iran (Stocklin 1968) or consider northern part of the Azerbaijan zone as including the Caucasus and Pontus Mountains in the Turkey (Innocenti et al. 1982). Figure 1 shows the location of the study area including the NTF as well as other active faults in East Azerbaijan (EA).

In this study, we detect fault segments based on a combination of the field studies and P–T dihedra analysis (Angelier and Mechler 1977) along the NTF. The essentials of this analysis (as beach balls and rose diagrams) give us a local paleostress distribution.

*Corresponding author.
E-mail address (es): pouya.sadeghi@rocketmail.com

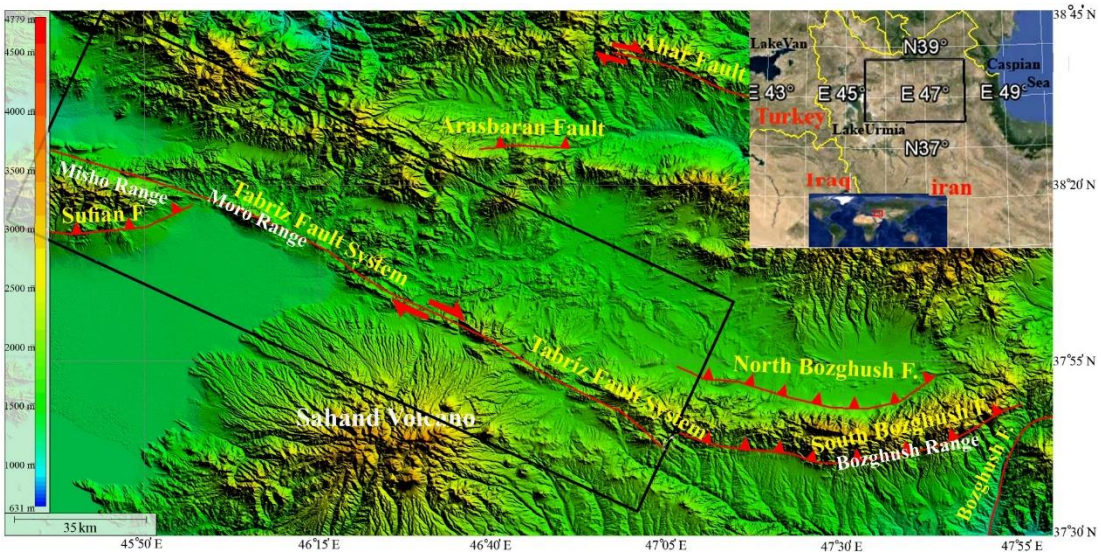

Fig 1. GTOPO30. Shaded relief image of the East Azerbaijan (EA) including main active faults. The small inset in the upper right corner represents the general location of EA, including the study area (the large oblique rectangle).

The stress distribution (Cowie and Shipton 1998, Duan and Oglesby 2006, Manighetti et al. 2007, Manighetti et al. 2015) and fault attitude (Zhang et al. 1999) change between the nearby tips of the segments. Therefore, using the azimuth and eigenvalue anomalies based on the presented methodology, we can find the areas suspected of segment boundaries. By specifying the number of segments forming the NTF, it is possible to take a new look at all the parameters under control of the segments, such as slip rates, compression and tension fields between the segments, and threats associated with the transverse faults.

2. Methodology

The fault segment boundaries in this study have been identified by locating anomalies associated with both of the azimuth distribution of faults and eigenvalues. Locations containing these anomalies are candidates for discontinuity along the fault strike. In practice, wherever the convergence or divergence of the eigenvalues and azimuth graphs occur together, there is a segmentation. In contrast, the absence of anomalies between the two consecutive measurement stations is indicative of fault continuity.

The NTF strikes N135°E over a length of more than 120 km, from the northwest of Sufian to the southeast of Bostanabad (Solaymani Azad et al. 2015) (Figs. 2 and 4). The attitude measurements have been performed for intervals of up to 5 km along the NTF. For each station, measurements were represented by rose and P–T dihedral diagrams, following the methodology applied by Angelier and Mechler (1977). P–T dihedra analysis has been shown as plots of eigenvalues versus distance from a reference location. The same plot has been used for azimuth distribution in terms of azimuth polarity obtained from rose diagrams. Among all stations, those with a distinct anomaly of azimuth distribution and eigenvalues were selected. Therefore, based on a simple statistical condition, data whose squared mean difference is greater than the standard deviation of the whole set have been chosen to be re-measured and plotted as graphs:

$$if: (x - \bar{x})^2 > \sigma \quad (1)$$

where x is the observed values of the sample item, $\bar{x}$ is the mean value of the observations, and σ is the sample standard deviation.

The stations with sharp anomalies of P–T dihedra analysis have been detected through scatter plots of eigenvalues and azimuth distribution along the NTF, versus the distance from the first measuring station located at Yam Ski resort. Finally, all anomalies have been verified by field measurements according to their location which is obtained from the eigenvalue and azimuth graphs. We have considered such locations as segment boundaries if there was evidence of transverse faults. It should be noted that the results published by other researchers have also been used to determine the exact attitude of the major faults.

3. Results

In this section we present the measurement anomalies together with the field observations that allowed us to identify the possible transverse faults intersecting the NTF. Figure 2 represents the locations of the P–T dihedra anomalies and Figure 3 shows the eigenvalue and azimuth polarity variations along the NTF.

The location of all the re-measured stations described below is shown in the Figure 4. The data collected in each measure station include all major and minor faults, where the latest are the ones that divide the NTF into segments, and located around the major ones.

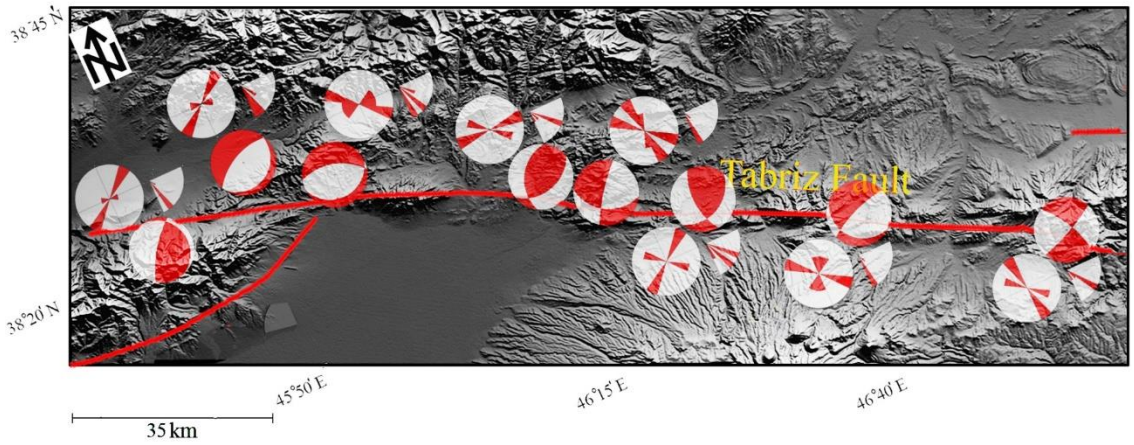

Fig 2. P–T dihedra diagrams for sites that are statistically distinct from other measure populations based on condition 1.

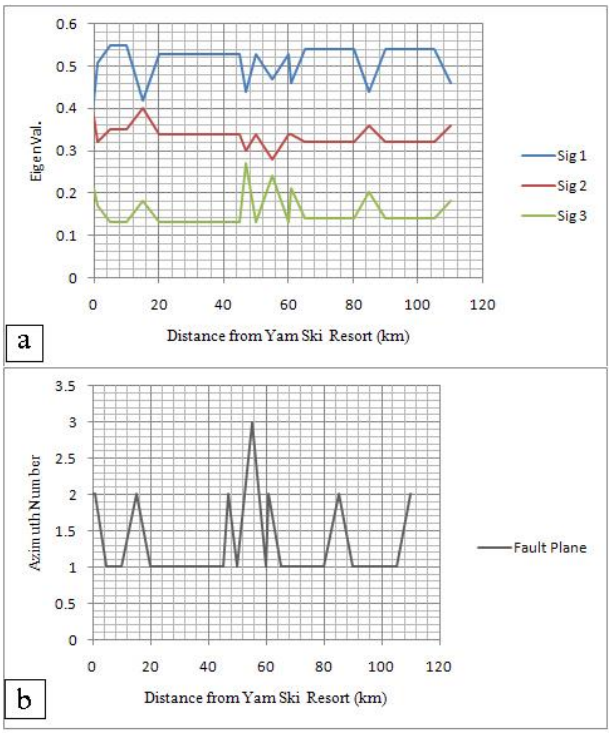

Fig 3. a) Scatter plots showing eigenvalue variations of stress tensors versus distance from the first measuring station. b) Variations of the measured fault azimuth number versus distance from the first measuring stations.

3.1. The Northwestern sector of the NTF

Based on the meizoseismal areas introduced by Hessami et al. (2003b), the part of the NTF located in the meizoseismal area of the 1780 AD events (except area common to the meizoseismal areas of the 1721 AD events) has been considered in this study as NW sector of the NTF. The NW sector of the NTF continues to the Misho range (Fig 5). The NW and SE terminations of the NTF are marked by the Mishu and Bozghush ranges, respectively (Solaymani Azad et al. 2015). The main suggested segmentation sites in this sector are as follows:

3.1.1. Yam Ski Resort site

The Ski Resort is near the Yam village, and 10 km far from southeast of Marand town (Fig 4). The juxtaposition of Quaternary deposits against Miocene units is obviously due to a minor normal faulting. Rose diagrams of all fault plane measurements show that minor strikes are more frequent than major ones. This valley fault intersects the NW sector of the NTF with an angle of ~45° (Fig 6).

3.1.2. Shor–Dareh site

Dip–direction of the NW sector of the NTF changes from NE to SW which is reflects an intersecting minor reverse fault around the Shor–Dareh village. This fault continues along the strike of the mentioned normal fault in the Ski resort site with the same strike and dip–direction. The main difference is the reverse dip component in Shor–Dareh site. The juxtaposition of the Quaternary and Neogene deposits is due to the reverse movement of this minor fault (Fig 7).

3.1.3. Sufian site

Around the intersection of the NTF and the Sufian fault (SF) located 5 km north of Sufian town (Fig 4), the NTF shows a different range of strike and dip–direction from those reported for NW and central sectors. In addition, there are minor fault planes in this site where the Sufian fault intersects the NTF. An outcrop of minor fault plane is close to the Andabil village and seems to be a trail of the Sufian fault intersecting the NTF (Fig 8).

3.2. The Central sector of the NTF

The part of the NTF that falls into the common zone of the meizoseismal areas (Hessami et al. 2003b) of the meizoseismal areas of the 1780 and 1721 AD events has been considered in this study as the central sector of the NTF. Most of the fault segmentation is around the central sector of the NTF next to Tabriz (Fig 4).

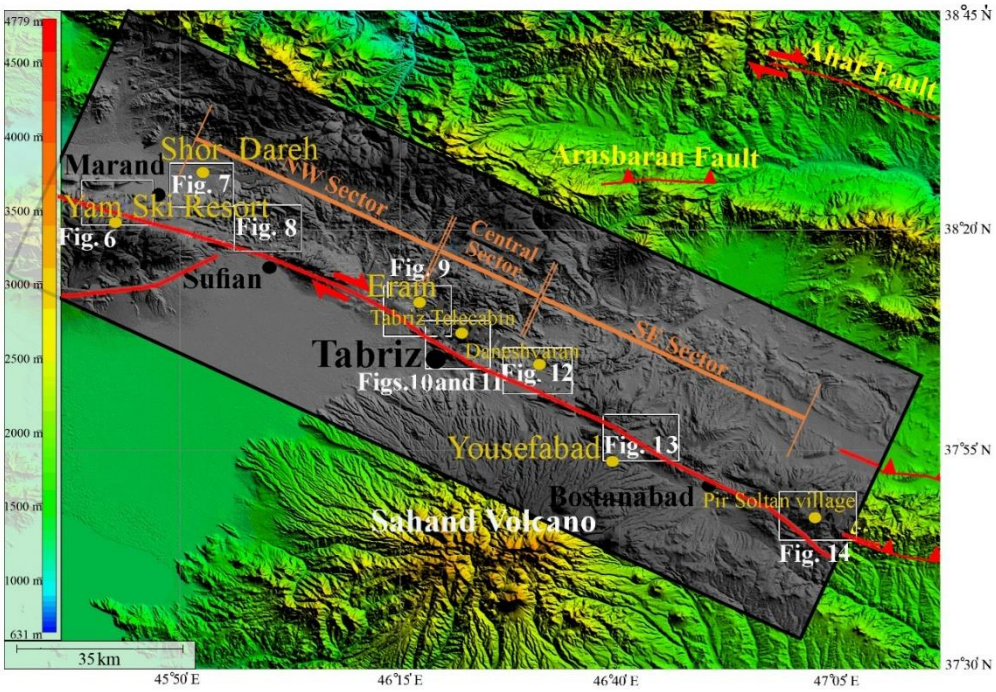

Fig 4. Digital Elevation Map (DEM) showing the measurement locations in the study area (gradient shaded area) around the North Tabriz Fault (NTF). The small insets represent the location of the figures of each measurement site. The black and yellow circles represent the nearest town or geographical area to the metering stations, respectively.

Fig 5. NW view of the NTF (red dashed line) continuing to the Misho range

Fig 6. Approximate location of transverse fault in the Yam Ski Resort site. a) Position of Yam Ski Resort fault (red triangles) to the NTF (red dashed line). b) The Angelier diagram showing orientation of fault planes (circles) and striae on fault surfaces (arrows).

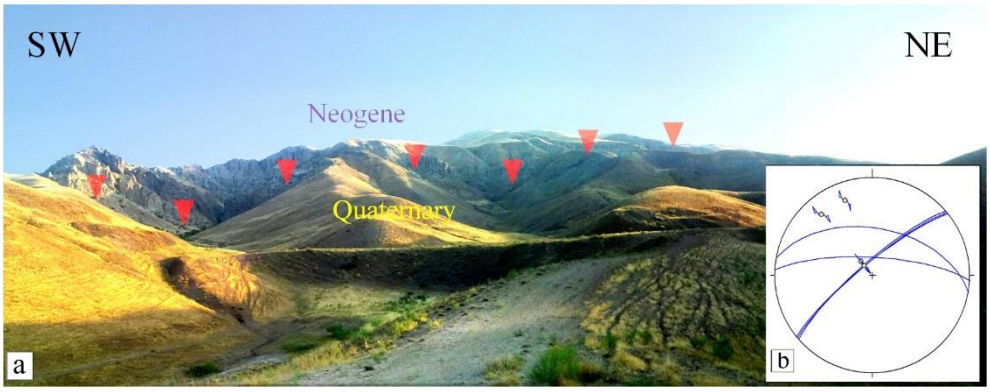

Fig 7. a) Approximate location of transverse fault in the Shor-Dareh site (red triangles). b) The Angelier diagram showing the orientation of fault planes (circles) and striae on fault surfaces (arrows)

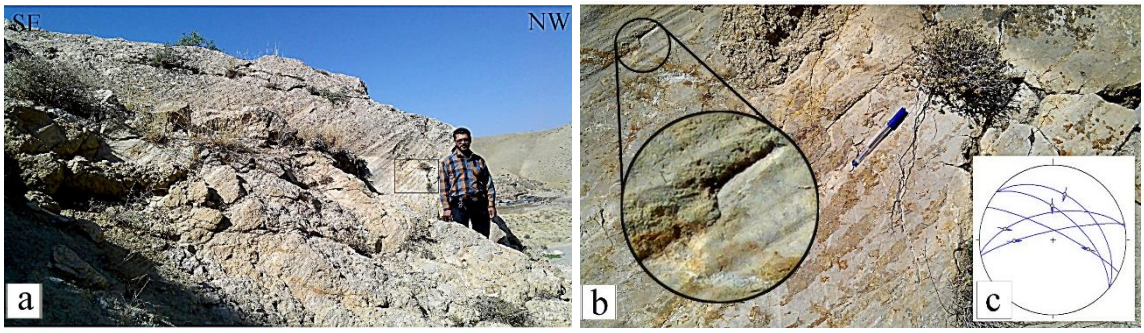

Fig 8. a) Compressional oblique–slip fault affecting Neogene conglomerates at the Sufian site. b) Close–up view of the rectangular area in (a) that shows the Andabil fault plane. c) The Angelier diagram showing the orientation of fault planes (circles) and striae on fault surfaces (arrows)

In this study, we only study the minor faults that are commensurate with the scale of the study area.

3.2.1. Eram site

A main discontinuity intersecting the central sector of the NTF has been observed close to the Eram turning in the eastern Tabriz beltway, which, according to the normal offset features, appears to be a minor normal fault (Fig 9a). The dip of the layers changes from almost horizontal in the regularly layered Miocene red beds to 44–65°SE. This structure appears to be due to the right step–over geometry and right–lateral strike–slip movements of the NTF on this site (Fig 9b).

3.2.2. Tabriz Telecabin site

A distinct difference in the dip–direction of the Miocene sequences on both sides of a new detected fault striking NNE–SSW around the Tabriz Telecabin (station 1) in the Einali range suggested that an Einali minor fault that intersects the NTF (Fig 10). The reverse movement of the NNE–SSW minor fault at second station of Telecabin (Fig 11a) represents a compressive field in this site. According to the dextral strike-slip faulting along the N135°E striking NTF, the compressive field between two segments in this site can be justified only by the left step–over geometry and right–lateral strike–slip movement of the NTF segments.

3.3. The Southeastern sector of the NTF

The part of the NTF located in the meizoseismal area (Hessami et al. 2003b) of the 1721 AD events (except area common to the meizoseismal areas of the 1780 AD events) has been considered in this study as SE sector of the NTF. The SE sector of the NTF continues to the South Bozghush range. The main suspected segmentation sites in this sector are as follows:

3.3.1. Daneshvaran site

Daneshvaran suburb is about 10 kilometers far from Tabriz. The normal component of the transverse fault cutting the main strike of the NTF represents the tension stress field. The juxtaposition of the Quaternary and Neogene red beds is due to the movement of this minor fault (Fig 12).

3.3.2. Bostanabad site

Around 50th km of the Tabriz–Bostanabad Highway, close to the Yousefabad village, a normal fault cuts across Pleistocene tuffs (Fig 13) and continues to the Holocene alluvial fans. Dip displacement seems to decrease from lower to upper layers in a nonlinear mode. Therefore, there is not any clear evidence on ground surface rupture whereas, the fault trace is obviously visible from the southern trench wall of the highway.

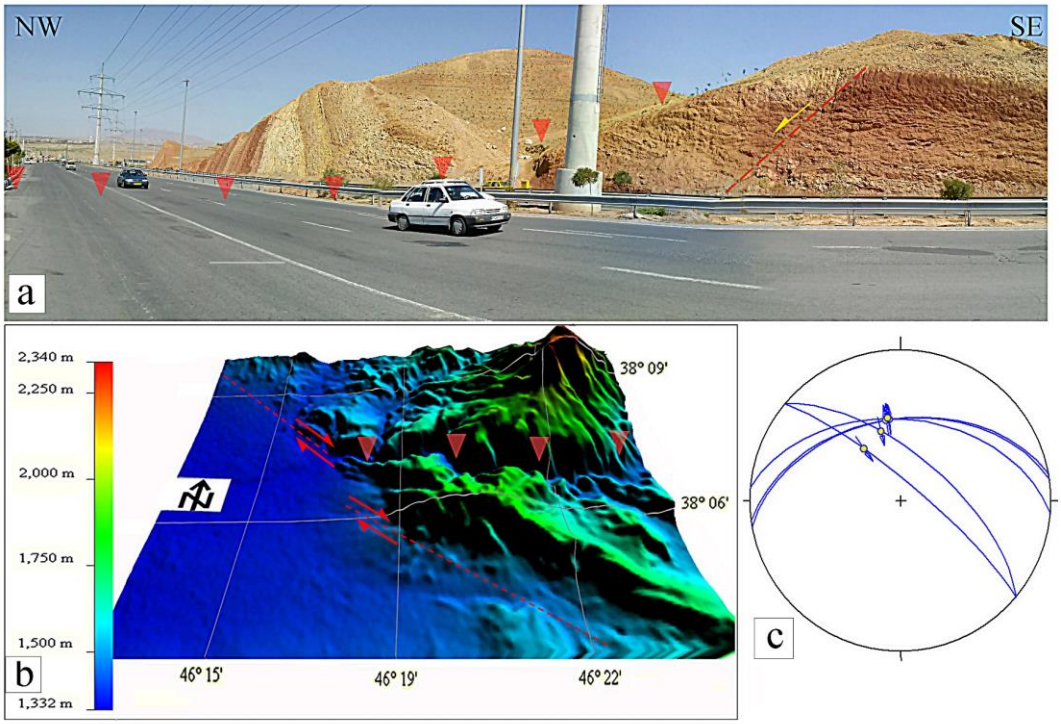

Fig 9. a) Difference in the dip direction of the Miocene sequences on both sides of the transverse fault (red triangles) in the Eram site. The normal fault (red dash line) represents the tension stress field in this region. b) A 3D Digital Elevation Model (DEM) representing the NTF segmentation by intersecting Eram transverse fault. c) The Angelier diagram showing the orientation of fault planes (circles) and striae on fault surfaces (arrows)

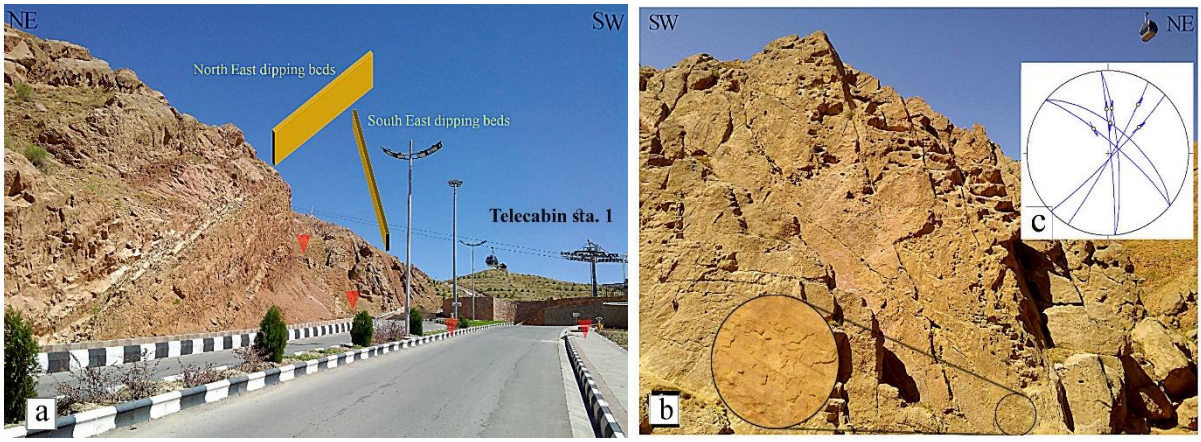

Fig 10. a) Difference in the dip direction of the Miocene sequences on both sides of the transverse fault (red triangles) in the Tabriz Telecabin site (station 1). b) Shear fractures on the mentioned transverse fault (Einali fault) plane. c) The Angelier diagram showing the orientation of fault planes (circles) and striae on fault surfaces (arrows)

3.3.3. South Bozghush site

The South Bozghush site is located close to the South Bozghush range, about 7 km to the NE of Bostanabad. A normal fault with right–lateral component cuts the Miocene formations. Based on the field observations, the fault outcrop is exposed on the edge of a topographical scarp close to the Pir Soltan village. The length of this transverse fault is about 15 km estimated at field observations, and the fault scarp is clearly evident in the Miocene deposits (Fig 14). Table 1 provides a general overview of the faults attitude of the study area based on the measurements performed in this study along with other references.

4. Discussion

The segmentation of the NTF fault system, is directly conditioned by the presence of minor faults that represents the main fault activity of the study area.

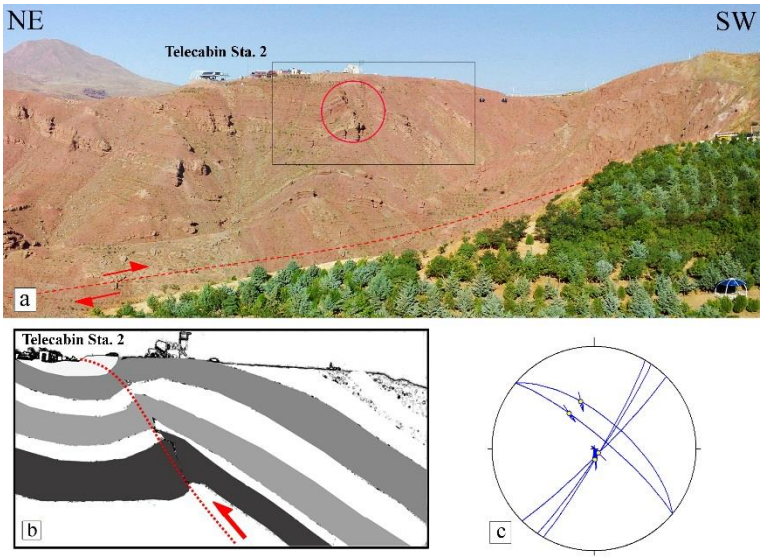

Fig 11. a) Reverse movement of Einali fault that intersects the NTF (red dash line) in the Tabriz Telecabin site (station 2). b) Sketch of the rectangular area in (a) representing the Einali fault (red dotted line) and the measurement location (red circle). c) The Angelier diagram showing the orientation of fault planes (circles) and striae on fault surfaces (arrows)

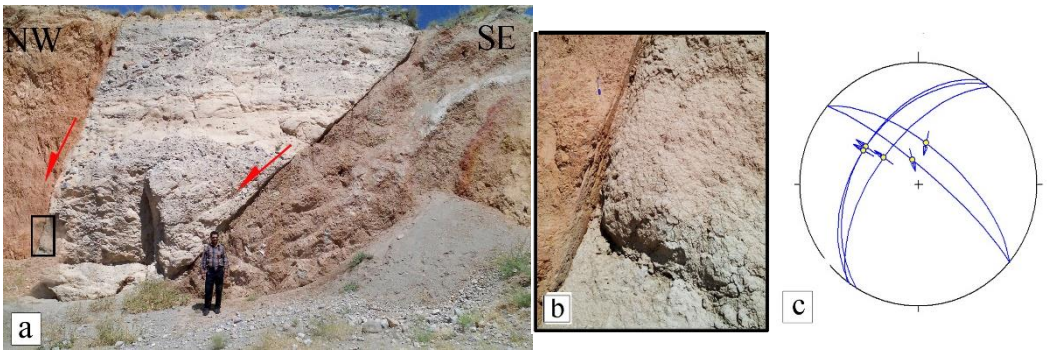

Fig 12. a) Juxtaposition of the Quaternary deposits and Neogene red beds by tension oblique-slip fault. b) Close-up view of the rectangular area in (a). c) The Angelier diagram showing the orientation of fault planes (circles) and striae on fault surfaces (arrows)

Table 1. Fault attitude data obtained from this study as well as from the other studies [a]

Fault Name	Length (km)	Strike	Dip	Mechanism	Min. Distance to the nearest city/town	Reference[b]
Yam Ski Resort	8	N045°	70° NW	Tensional Oblique–slip	Yam	
Shor–Dareh	8	N050°	80° NW	Compressional Oblique–slip	Yam	
Andabil	16	N080°	80° NW	Right lateral Strike–slip, Reverse component	Sufian	
Sufian	47	N085°	60°–80° NW	Right lateral Strike–slip, Reverse component	Sufian	Berberian and Yeats 1999; Karakhanian *et al.* 2004; Ghahremani 2010.
NTF (North West)	70	N120°	70°–90° NE	Right lateral Strike–slip, Reverse component	Tabriz	Ambraseys and Melville 1982; Berberian and Yeats 2001; Hessami *et al.* 2003a; Karakhanian *et al.* 2004; Solaymani Azad 2009, Rizza 2010; Fathian Baneh 2011; Ritz *et al.* 2011.
Eram	20	N085°	45° NW	Tensional Oblique–slip	Tabriz	
Tabriz Telecabin	7	N005°	85° SE	Compressional Oblique–slip	Tabriz	
Daneshvaran	8	N045°	80° NW	Tensional Oblique–slip	Daneshvaran Suburb	
Yousefabad	10	N010°	80° SE	Normal, Right lateral Strike–slip component	Bostanabad	
NTF (South East)	85	N120°	40°–60° NE	Thrust	Zanjan	Hessami *et al.* 2003a.
Pir Soltan	12	N010°	50° NE	Tensional Oblique–slip	Bostanabad	

[a]Data from publications by other researchers are only about the NTF whereas the measured data in this work are related to the minor intersecting (transverse) faults. [b]Only data from other publications are filled in.

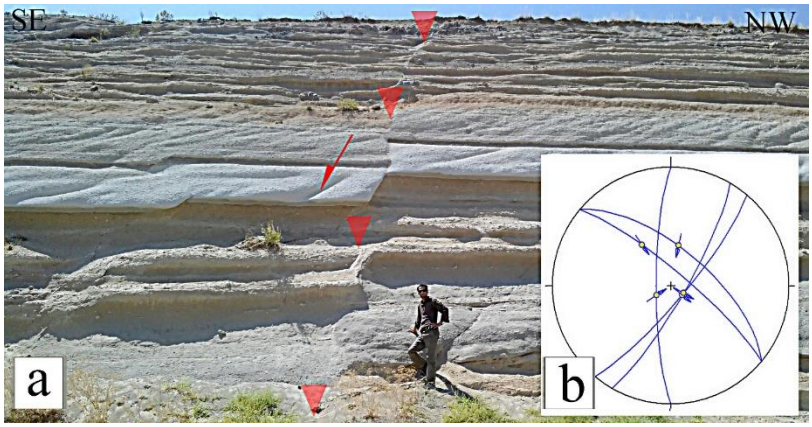

Fig 13. Approximate location of transverse fault in Bostanabad site. a) Yousefabad normal fault cuts across Pleistocene tuffs (red triangles). b) The Angelier diagram showing the orientation of fault planes (circles) and striae on fault surfaces (arrows)

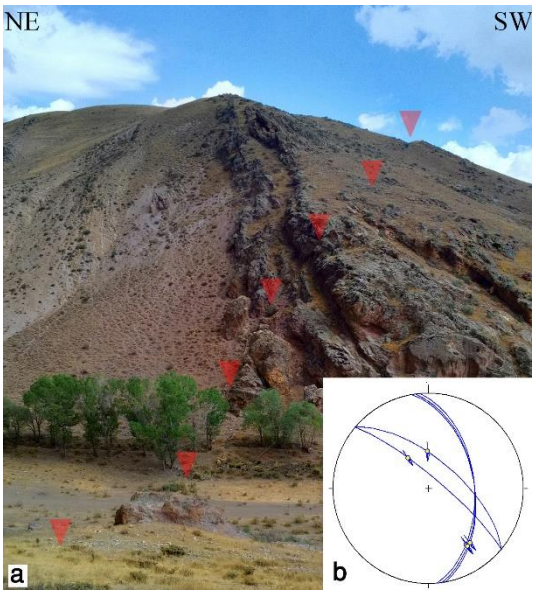

Fig 14. Approximate transverse fault location in South Bozghush site. a) Pir Soltan Tensional oblique-slip fault cuts across Miocene deposits (red triangles). b) The Angelier diagram showing the orientation of fault planes (circles) and striae on fault surfaces (arrows)

P–T dihedra and azimuth distribution anomalies show ~7 picks in their scatter plots (Fig 3). Figures 3a and 3b represent that anomalies are distributed in all three sectors of the NTF. Finally, locations with quadri-anomalies have been verified by field measurements (Fig 4). Field observations in the Results section confirm that pick locations are in accordance with transverse faults. Fault attitude data obtained from field observations in this study as well as from the other studies were shown in the Table 1. The introduced stations represent the sites that transverse faults are passing from. These transverse faults include Yam Ski Resort, Shor–Dareh, Andabil, Eram, Einali, Daneshvaran, Yousefabad, and Pir–Soltan (Table 1).

Therefore, we provided an outline representing the main segments of the NTF based on the locations and attitudes of the major transverse faults (Fig 15). According to the results, of the 7 transverse faults that surround 6 segments, two of them are in the NW sector, three in the central sector, and the other two in the SE Sector of the NTF. In addition, the shortest and longest segment lengths are ~6 km and ~31 km, respectively (Fig 15b). The outline represents that small segments are in central sector and big segments surrounding them on both sides in NW and SE sectors. The minor faults of the Yam Ski Resort and Shor–Dareh structurally seem to be related together. The continuity of the Yam Ski Resort and the Shor–Dareh faults along the same strike but different dip-slip components indicate the probability of rotational motions of the transverse fault at the time of segmentation. However, this statement needs further study. The left and right step–over geometries of the NTF segments leads to tensile and compressive stress fields, respectively. According to the schematic outline shown in Figure 15, most of the compressive stress fields appear to be located in the NW sector and tensile stress fields in the SE sector of the NTF.

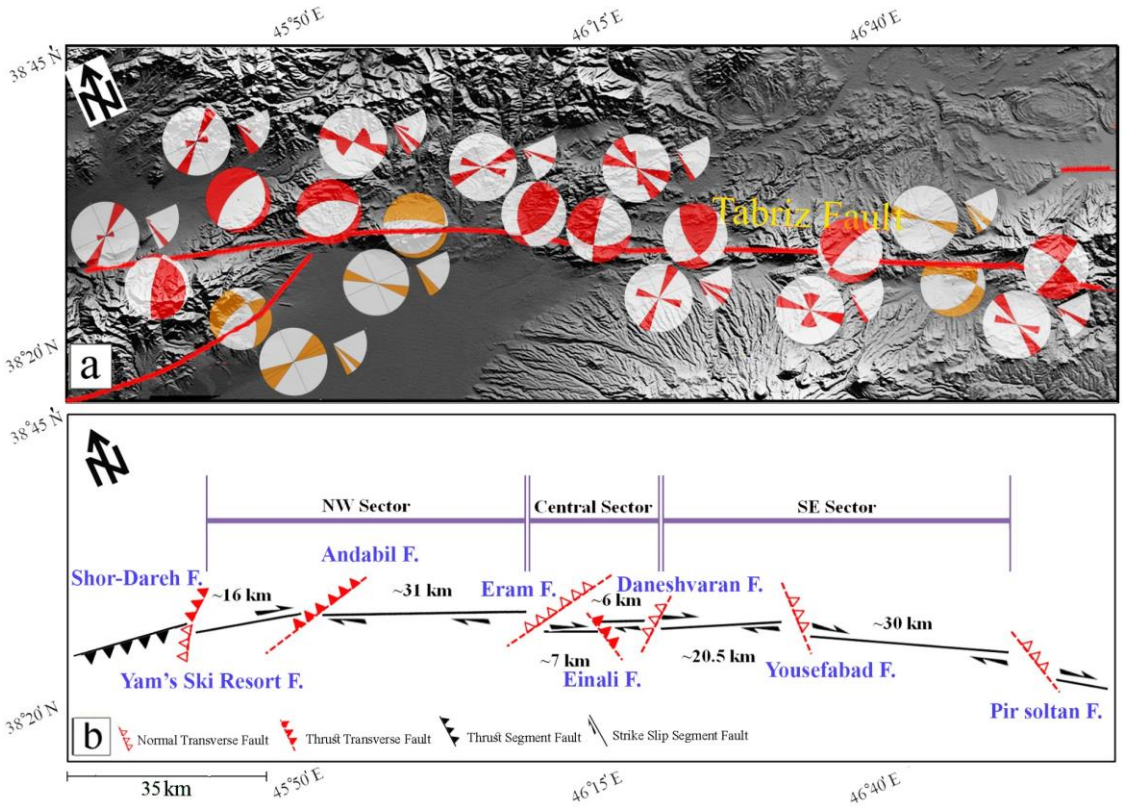

Fig 15. a) P-T dihedra diagrams as well as strike and dip azimuth plotted for each site. Red and orange beach balls relate to observations and other references mentioned in Table 1, respectively. b) A schematic outline representing the main transverse faults and segments of the NTF detection based on P–T dihedral analysis and field observations

Most of the introduced transverse faults showed a good agreement with the mechanisms related to the convergent and divergent steps (Fig 10). The arrangement of the introduced transverse faults is such that it corresponds to the areas affected by subsidence (e.g. Rizza et al. 2013) in the south of the Tabriz fault. While confirming previous findings (Berberian 1997, Karakhanian et al. 2004), the results of this study introduce new segments along the NTF. The number of segments forming the NTF gives the idea that this fault has different slip rates along its length, which, despite assuming a specific slip rate, could be the start of new studies in this regard.

5. Conclusions

The segments detected based on P–T dihedra analysis suggests the eigenvalue and azimuth distribution anomalies as important items that are controlled by discontinuities along the major fault. The anomalies indicate that there are six main segments per three sectors of the NTF. In addition, each segment was bounded on its terminations by two transverse faults. This study also show that the stress fields between the NTF segments are often compressive in the NW sector and tensile in the SE sector. However, our results confirm earlier reported segments, but introduce new segments along the NTF. The future works include the numerical analysis of the earthquakes related to the NTF and comparing the results with those obtained from P–T dihedra analysis.

6. Acknowledgements

We thank the General Governor Office and Department of Roads and Urban Development of East Azerbaijan who shared their information and knowledge about access routes of EA.

7. References

Amadei B, Stephansson O (1997) Rock stress and its measurement. *Springer Science & Business Media*.

Ambraseys NN, Melville CP (2005) A history of Persian earthquakes. Cambridge University press.

Angelier J, Mechler P (1977) Sur une methode graphique de recherche des contraintes principales egalement utilisable en tectonique et en seisrnoloqie: la methode des diedres droits, *Bulletin de la Société Géologique de France* 19:1309-1318.

Berberian M (1997) Seismic sources of the Transcaucasian historical earthquakes. Historical and prehistorical earthquakes in the Caucasus, *Kluwer Academic Press* 28: 233-311.

Berberian M, Yeats RS (1999) Patterns of historical earthquake rupture in the Iranian Plateau, *Bulletin of the Seismological society of America* 89(1): 120-139.

Berberian M, Yeats RS (2001) Contribution of archaeological data to studies of earthquake history in

the Iranian Plateau, *Journal of Structural Geology* 23(2): 563-584.

Cowie PA, Shipton ZK (1998) Fault tip displacement gradients and process zone dimensions, *Journal of Structural Geology* 20(8): 983-997.

de Joussineau G, Aydin A (2009) Segmentation along strike–slip faults revisited, *Pure and Applied Geophysics* 166(10): 1575-1594.

Duan B, Oglesby DD (2006) Heterogeneous fault stresses from previous earthquakes and the effect on dynamics of parallel strike-slip faults, *Journal of Geophysical Research: Solid Earth* 111(B5).

Fathian Baneh A (2011) Paleoseismological investigations along the North Tabriz Fault: [Dissertation]. Islamic Azad University, Tehran. 100–120. (in Persian)

Faulds JE, Coolbaugh MF, Vice GS, Edwards ML (2006) Characterizing structural controls of geothermal fields in the northwestern Great Basin: A progress report. *Geothermal Resources Council Transactions* 30:69-76.

Faulds JE, Moeck I, Drakos P, Zemach E (2010) Structural assessment and 3D geological modeling of the Brady's geothermal area, Churchill County (Nevada, USA): a preliminary report. In Proc. 35th Workshop on Geothermal Reservoir Engineering, *Stanford University, Stanford*, CA, SGP-TR-188.

Ghahremani A (2010) Morphotectonic investigations along the Shabestar Fault: [Dissertation]. Islamic Azad University, Tehran. 80–90. (in Persian)

Hessami K, Jamali F, Tabassi H (2003a). Major active faults of Iran. International Institute of Earthquake Engineering and Seismology, scale 1:250,000.

Hessami K, Pantosti D, Tabassi H, Shabanian E, Abbassi MR, Feghhi K, Solaymani S (2003b). Paleoearthquakes and slip rates of the North Tabriz Fault, NW Iran: *preliminary results. Annals of Geophysics* 46(5).

Huenges E (2010) Deployment of Enhanced Geothermal Systems Plants and CO_2 Mitigation. Geothermal energy systems–Exploration, development and utilization. 1st. edition. Wiley-VCH.

Innocenti F, Manetti P, Mazzuoli R, Pasquare G, Villari L (1982) Anatolia and north–western Iran. *Andesites: Orogenic andesites and related rocks:* 327–349.

Karakhanian AS, Trifonov VG, Philip H, Avagyan A, Hessami K, Jamali F, Bayraktutan MS, Bagdassarian H, Arakelian S, Davtian V, Adilkhanyan A (2004) Active faulting and natural hazards in Armenia, eastern Turkey and northwestern Iran, *Tectonophysics* 380(3): 189-219.

Mandl G (1999) Faulting in brittle rocks: an introduction to the mechanics of tectonic faults. Springer–Verlag.

Manighetti I, Campillo M, Bouley S, Cotton F (2007) Earthquake scaling, fault segmentation, and structural maturity, *Earth and Planetary Science Letters* 253(3): 429-438.

Manighetti I, Caulet C, Barros L, Perrin C, Cappa F, Gaudemer Y (2015) Generic properties of the fault lateral segmentation: Implications on fault growth, stress heterogeneity, and earthquake dynamics, *Geochemistry Geophysics Geosystems* 16(2): 443-467.

Manighetti I, Zigone D, Campillo M, Cotton F, (2009) Self–similarity of the largest–scale segmentation of the faults: Implications for earthquake behavior, *Earth and Planetary Science Letters* 288(3): 370-381.

Mansfield C, Cartwright J (2001) Fault growth by linkage: observations and implications from analogue models, *Journal of Structural Geology* 23(5): 745-763.

Nabavi MH, (1976) An introduction to the Iranian geology. *Geological Survey of Iran, Tehran*. Report 3: 110. (in Persian)

Nelson R (2001) Geologic analysis of naturally fractured reservoirs. *Elsevier*.

Pollard DD (2000) Strain and stress: discussion, *Journal of Structural Geology* 22(9): 1359-1367.

Ritz JR, Rizza M, Vernant P, Peyret M, Nazari H, Nankali H, Djamour Y, Mahan S, Salamati R, Tavakoli F (2011). Morphotectonics and geodetic evidences for a constant slip-rate along the Tabriz Fault (Iran) during the past 45 kyr. *In AGU Fall Meeting Abstracts*.

Rizza M (2010) Analyses des vitesses et des déplacements cosismiques sur des failles décrochantes en Mongolie et en Iran: approche morphotectonique et paléosismologique: [Dissertation]. *University of Montpellier 2, Montpellier*: 200–220. (in French)

Rizza M, Vernant P, Ritz JF, Peyret M, Nankali H, Nazari H, Djamour Y, Salamati R, Tavakoli F, Chery J, Mahan SA (2013). Morphotectonic and geodetic evidence for a constant slip-rate over the last 45 kyr along the Tabriz fault (Iran). *Geophysical Journal International*, *193*(3): 1083-1094.

Sadeghi-Farshbaf P, Khatib MM, Nazari H (2019) Future stress accumulation zones around the main active faults by 3D numerical simulation in East Azerbaijan Province, Iran. *Acta Geodaetica et Geophysica* 54(4): 461-481.

Solaymani Azad S (2009) Evaluation de l'aléa sismique pour les villes de Téhéran, Tabriz et Zandjan dans le NW de l'Iran. Approche morphotectonique et paléosismologique: [Dissertation]. *University of Montpellier 2, Montpellier*. 100–150. (in French)

Solaymani Azad S, Philip H, Dominguez S, Hessami K, Shahpasandzadeh M, Foroutan M, Tabassi H, Lamothe M (2015) Paleoseismological and morphological evidence of slip rate variations along the North Tabriz fault (NW Iran), *Tectonophysics* 640: 20–38.

Stocklin J (1968) Structural history and tectonics of Iran: a review, *AAPG Bulletin* 52(7): 1229-1258.

Trudgill B, Cartwright J (1994) Relay–ramp forms and normal–fault linkages, Canyonlands National Park, Utah, *Geological Society of America Bulletin* 106(9): 1143-1157.

Walsh JJ, Watterson J (1991) Geometric and kinematic coherence and scale effects in normal fault systems, *Geological Society, London, Special Publications* 56(1): 193-203.

Whipp PS, Jackson CL, Schlische RW, Withjack MO, Gawthorpe RL (2016) Spatial distribution and evolution of fault–segment boundary types in rift systems: observations from experimental clay models, *Geological Society, London, Special Publications* 439: SP439-7.

Zhang P, Mao F, Slemmons DB (1999) Rupture terminations and size of segment boundaries from historical earthquake ruptures in the Basin and Range Province, *Tectonophysics* 308(1): 37-52.